Chinese Chemical Letters 34 (2023) 107950

Contents lists available at ScienceDirect

Chinese Chemical Letters

journal homepage: www.elsevier.com/locate/cclet

Generation of color-controllable room-temperature phosphorescence *via* luminescent center engineering and *in-situ* immobilization

Licheng Zheng[a], Kai Jiang[a,*], Jiaren Du[a], Yike Li[b], Zhongjun Li[b], Hengwei Lin[a,*]

[a] *International Joint Research Center for Photo-responsive Molecules and Materials, School of Chemical and Material Engineering, Jiangnan University, Wuxi 214122, China*

[b] *College of Chemistry and Molecular Engineering, Zhengzhou University, Zhengzhou 450001, China*

ARTICLE INFO

Article history:
Received 6 August 2022
Revised 17 October 2022
Accepted 23 October 2022
Available online 28 October 2022

Keywords:
Carbon dots
Room-temperature phosphorescence
Luminescent center engineering
In-situ immobilization
Anti-counterfeiting
Information security

ABSTRACT

Materials with controllable luminescence colors are highly desirable for numerous promising applications, however, the preparation of such materials, particularly with color-controllable room-temperature phosphorescence (RTP), remains a formidable challenge. In this work, we reported on a facile strategy to prepare color-controllable RTP materials *via* the pyrolysis of a mixture containing 1-(2-hydroxyethyl)-urea (H-urea) and boric acid (BA). By controlling the pyrolysis temperatures, the as-prepared materials exhibited ultralong RTP with emission colors ranging from cyan, green, to yellow. Further studies revealed that multiple luminescent centers formed from H-urea, which were *in-situ* embedded in the B_2O_3 matrix (produced from BA) during the pyrolysis process. The contents of the different luminescent centers could be regulated by the pyrolysis temperatures, resulting in color-tunable RTP. Significantly, the luminescent center engineering and *in-situ* immobilization strategy not only provided a facile method for conveniently preparing color-controllable RTP materials, but also endowed the materials prepared at relatively lower temperatures with color-changeable RTP features under thermal stimulus. Considering their unique properties, the potential applications of the as-obtained materials for advanced anti-counterfeiting and information encryption were preliminarily demonstrated.

Manipulating the emission colors of luminescent materials has attracted tremendous attention due to significant applications in many fields, such as colorful displays, polychrome anti-counterfeiting, multi-color bioimaging, and multiplexed sensing [1–8]. Among the different types of luminescent materials, room-temperature phosphorescent (RTP) materials are considered more attractive for practical applications, especially for applications requiring high-difficulty of forging, high signal-to-noise ratio sensing, and high resolution of time-resolved bioimaging [9–14], due to their long persistent emission features. To overcome the drawbacks of traditional inorganic RTP materials based on transition metals and rare-earth ions, which have harsh preparation conditions and scarcity of rare-earth resources, special attention has been paid to the exploitation of metal-free RTP materials over the last few decades [15,16]. Therefore, the regulation of RTP colors from pure organic materials has been regarded as a critical issue [17]. In general, the generation of RTP requires efficient spin-orbit coupling (SOC) to populate triplet excitons by facilitating the intersystem crossing (ISC) process while also suppressing their non-radiative decay by stabilizing the excited triplet species [18–20]. Of note, an increasing number of organic materials with colorful RTP have recently been developed by modulating their chemical structures based on molecular engineering, followed by stabilizing their triplet states through crystallization, aggregation, and/or embedding in matrices [15,16,18,21-23]. However, organic small molecule-based RTP materials often suffer from complicated synthesis and purification processes, and have difficulty achieving controllable RTP colors. Therefore, the development of facile strategies for preparing metal-free RTP materials with controlled emission color is still desirable, but highly challenging. In addition, it is also very significant to develop color-changeable metal-free RTP materials under external stimuli [24–26]. The preparation of these materials is a more challenging task, because it is necessary to simultaneously satisfy the general requirements for producing RTP and change the emission colors *via* an external stimulus. To the best of our knowledge, such materials have rarely been reported until now [27,28].

Recently, carbon dots (CDs) have attracted significant attention for the construction of tunable luminescent materials due to their

* Corresponding authors.
E-mail addresses: jiangkai@jiangnan.edu.cn (K. Jiang), linhengwei@jiangnan.edu.cn (H. Lin).

https://doi.org/10.1016/j.cclet.2022.107950
1001-8417/

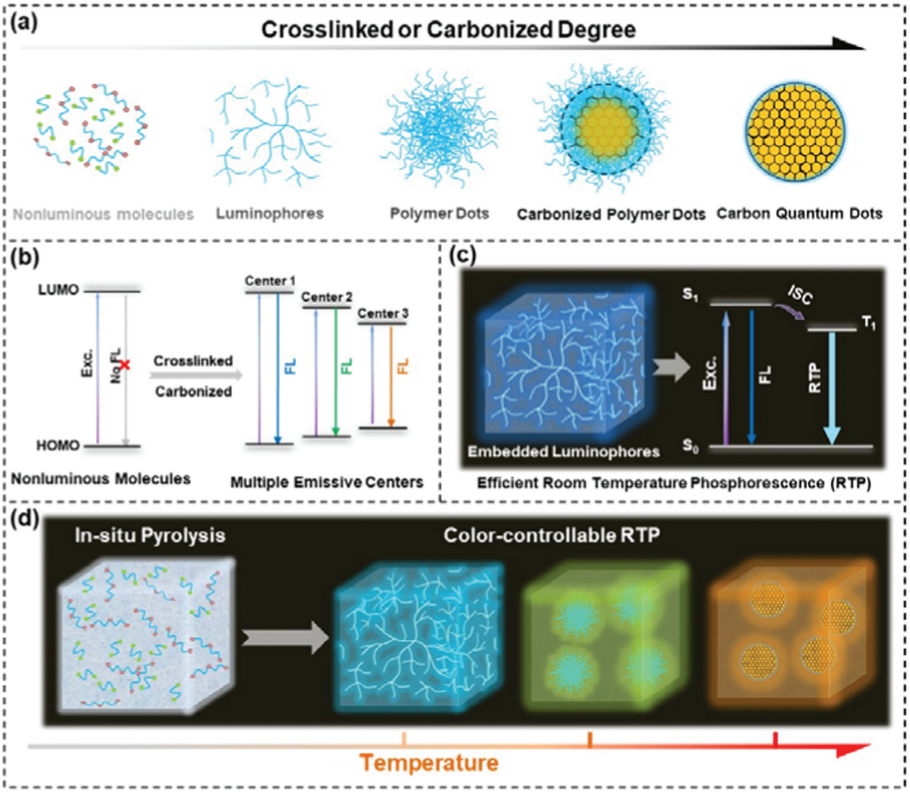

Fig. 1. Schematic representation of the luminescent center engineering and *in-situ* immobilization process. (a) Schematic illustration the conversion process from nonluminous molecules into luminophores, polymer dots, carbonized polymer dots and carbon quantum dots with increased reaction temperature (or carbonization degree). (b) Generation of multiple emissive centers from nonluminous molecules due to the crosslink enhanced emission (CEE) effect. (c) Schematic illustration the activation of RTP from nonconventional luminophores after they were embedded in solid matrices. (d) Proposed process for achieving multi-color RTP *via in-situ* pyrolysis of mixed carbon sources and matrix precursors under different temperatures.

facile preparation, high photostability, and outstanding biocompatibility [29,30]. More impressively, CDs-based stimuli-responsive luminescent materials had also been exploited in recent years. Particularly, both wang's group and Ding's group achieved CDs-based multicolor RTP across a broad range of visible-light region by adjusting fabrication temperature and/or starting materials [31,32]. These studies opened new sights for preparing stimuli-responsive RTP materials, but a general design principle/strategy to prepare such CDs-based materials is still necessary and significant. Generally, multicolor emissions from CDs, regardless of photoluminescence (PL) or RTP, has benefited from their multiple emitting centers, therefore, the emissions of CDs can be facilely regulated by luminescent centers engineering. Specifically, the phenomenon of crosslink enhanced emission (CEE) has been accepted as one of the possible PL origins of CDs prepared from nonluminous organic small molecules [33,34]. Accordingly, the CEE process can be regarded as the most typical example of CD luminescent center engineering. During the formation of CDs, nonconventional luminophores form first and gradually convert into polymer dots, carbonized polymer dots, and finally carbon quantum dots (abbreviated as PDs, CPDs, and CQDs, respectively, which consist of the three types of CDs with different phases structures) with increased reaction temperature (or carbonization degree) (Fig. 1a), resulting in multiple luminescent centers and tunable PL emission (Fig. 1b) [35–37]. Notably, strong RTP with a long duration can be obtained from organic nonconventional luminophores embedded in a matrix due to the suppression of non-radiative transitions through the efficient confinement of molecular vibrations and motion (Fig. 1c) [38,39]. Inspired by the concept of CEE and efficient RTP from nonconventional luminophores embedded in matrices, we speculated that it might be possible to realize controlled multicolor RTP by the *in-situ* pyrolysis of suitable carbon and matrix precursors (Fig. 1d). Similar to the preparation of CEE-type CDs (CEE-CDs) from nonluminous organic small molecules, nonconventional luminophores with multiple luminescent centers can be obtained and *in-situ* embedded in a rigid matrix. In our recent work, we confirmed that multiple emissive centers could be reserved along with the further carbonization of CEE-CDs under relative higher temperatures (*e.g.*, 240–300 °C), where the content of the different centers was temperature-dependent [40]. We reasoned that with the selection of appropriate precursors and pyrolysis temperatures, the RTP colors of the corresponding materials could be controlled. More impressively, this pyrolysis and *in-situ* luminescent center immobilization strategy could provide a facile approach for obtaining color-changeable RTP materials under thermal stimulus, which has rarely been reported.

To validate our hypothesis, 1-(2-hydroxyethyl)-urea (H-urea) and boric acid (BA) were screened as the starting materials according to the following considerations. (i) H-urea could act as a carbon source that could produce abundant C=O and C=N groups, and these groups were confirmed to be critical for producing RTP from organic materials [41–43]. (ii) The dehydration of BA produced boric oxide (B_2O_3), which could act as a matrix to *in situ* embed the produced luminescent species, thus, suppressing non-radiative transitions of their triplet states [31,44,45]. (iii) The dehydration and condensation between BA and H-urea would form covalent bonds, which could further stabilize the triplet states and alter their energy levels [31,44,45]. (iv) The introduction of B and N could promote $\pi \rightarrow \pi^*$ and $n \rightarrow \pi^*$ transitions and populate triplet states by facilitating the ISC process for the generation

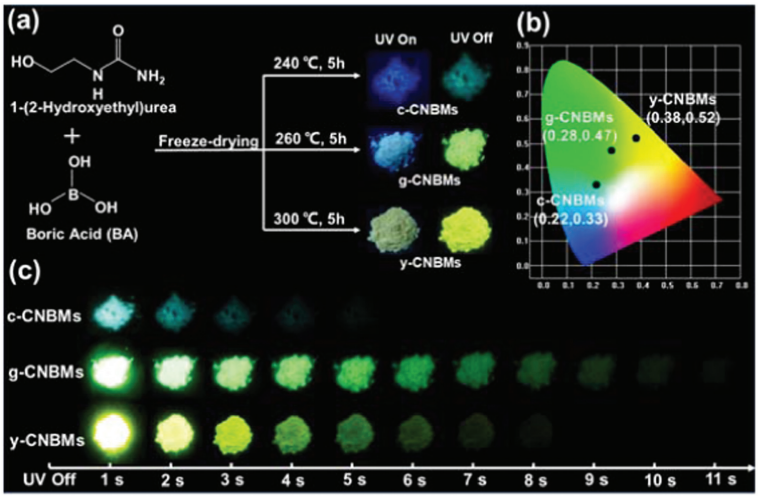

Fig. 2. Preparation process and afterglow performance. (a) Schematic illustration for the preparation for multi-color RTP composites (denoted as c-CNBMs, g-CNBMs and y-CNBMs, respectively) *via* a direct pyrolysis method at different temperatures. (b) Calculated CIE coordinates from the afterglow spectra ($\lambda_{ex} = 365$ nm) of c-CNBMs, g-CNBMs, and y-CNBMs. (c) Afterglow emission images of the three RTP composites after ceasing UV lamp (365 nm) irradiation from 1 s to 11 s under ambient conditions.

of RTP [23,46,47]. In addition, (v) the vacant p orbitals of the B atoms could interact with the $\pi \rightarrow \pi^*$ and $n \rightarrow \pi^*$ transitions of the C=O and C=N groups, triggering the generation of through-space conjugation (TSC) emission [38], which could serve as a luminescent center to regulate and expand RTP colors. As a proof of concept, direct pyrolysis of the BA and H-urea mixture under different temperatures (*i.e.*, 240, 260 and 300 °C) was performed and we systematically characterized the structural and photophysical properties of the obtained materials. As anticipated, the obtained three materials were phosphorescent with a relatively long afterglow duration under ambient conditions (5∼11 s), exhibiting controlled RTP colors from cyan, green, to yellow at different pyrolysis temperatures. Further analysis revealed that multiple luminescent centers formed and were embedded *in-situ* in the B_2O_3 matrix during the pyrolysis process. In addition, the contents of the different centers were controlled by the pyrolysis temperatures; thus, triggering the color-tunable RTP. Interestingly, the materials prepared at relatively lower temperatures (*e.g.*, 240 °C) exhibited a rarely reported thermo-stimuli-responsive color-changeable RTP feature. Finally, the potential uses of these materials in advanced anti-counterfeiting and information encryption were demonstrated. This study not only developed a facile strategy for the convenient preparation of RTP materials and the controllable regulation of their emission color, but also provided a novel idea for designing and preparing thermo-stimuli-responsive smart materials.

As shown in Fig. 2a, the materials with a color-tunable afterglow were prepared by the direct pyrolysis of an H-urea and BA mixture at 240, 260 and 300 °C (see details in the experimental section in Supporting information). Upon UV (365 nm) excitation, the as-obtained materials exhibited deep blue, cyan, and yellow-green fluorescence (FL), respectively. Interestingly, cyan, green, and yellow afterglows were observed from the three materials (denoted as c-CNBMs, g-CNBMs, and y-CNBMs, respectively), after the excitation source was turned off. According to the afterglow emission spectra (Fig. S1 in Supporting information), the CIE coordinates of their afterglow emissions under 365 nm of excitation were calculated to be (0.22, 0.33), (0.28, 0.47) and (0.38, 0.52) (Fig. 2b), which was consistent with the afterglow colors observed by the naked eye. Of note, the afterglow intensities of all the materials showed apparent decreases with increasing measurement temperatures (Fig. S2 in Supporting information), suggesting phosphorescent emission characteristics [19,23]. Moreover, the afterglow emissions of the c-CNBMs, g-CNBMs, and y-CNBMs could be observed by the naked eye for *ca.* 5 s, 11 s and 8 s, respectively (Fig. 2c and Videos S1–S3 in Supporting information). Obviously, the duration of the afterglow emissions was also dependent on the pyrolysis temperature.

Subsequently, the morphologies and structures of these materials were characterized by transmission electron microscopy (TEM), energy dispersive X-ray spectroscopy (EDS), and X-ray diffraction (XRD) analysis. As shown in Fig. S3 (Supporting information), the TEM and high-resolution TEM (HR TEM) images showed that the highly crystallized nanoparticles were well-dispersed and embedded in the y-CNBMs, which was attributed to the formation of CQDs, according to the observed lattice spacing. However, only amorphous particles (likely CPDs) were observed in the g-CNBMs and no obvious particle structures were found in the c-CNBMs (Figs. S4 and S5 in Supporting information). Therefore, we tentatively attributed the PL of the c-CNBMs, g-CNBMs, and y-CNBMs to the temperature-dependent formation of nonconventional luminophores, CPDs, and CQDs. Notably, the uniform distribution of B, C, N and O elements in the EDS elemental mappings verified that all of the elements were well distributed. This situation may have promoted the probability of interactions between the empty p orbitals on the B atoms and the lone pair electrons provided by N and O, which was beneficial for the TSC process [38]. Compared to BA treated at 260 °C, the XRD patterns of c-CNBMs, g-CNBMs, and y-CNBMs presented the characteristic peaks of B_2O_3 at 14.68°, 28.05°, 30.77° and 40.35° (Fig. 3a) [48]. Phosphorescence is typically quenched in the presence of oxygen and solvents owing to the quenching of triplet excitons and solvent-assisted relaxation [19,23]. Therefore, embedding fluorophores and CDs in a solid matrix is generally needed for activating phosphorescence emission [49–51]. Since no afterglow was observed in the aqueous dispersions of these materials, the formation of B_2O_3 as a matrix was considered to be critical for RTP emissions.

To gain insight into the formation process of these materials, their chemical structures were investigated by Fourier-transform infrared (FT-IR) spectroscopy and X-ray photoelectron spectroscopy (XPS), and then carefully compared with B_2O_3. As shown in Fig. 3b, the FT-IR spectrum of B_2O_3 displayed characteristic absorption bands at 3210 cm^{-1}, 1457 cm^{-1}, and 1195 cm^{-1}, which was attributed to the stretching vibrations of O – H and B – O bonds [31,44], and asymmetrically stretched oxygen atoms [38], which connected the trigonal boron atoms, respectively. For the FT-IR spectra of c-CNBMs, g-CNBMs, and y-CNBMs, the peak assigned to

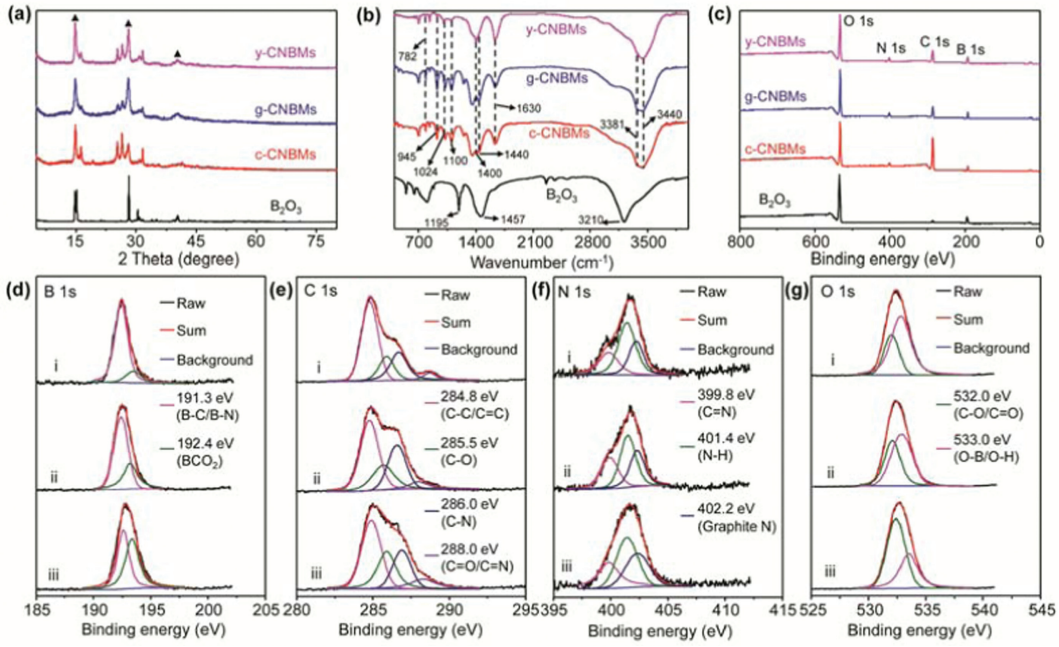

Fig. 3. Chemical structures analysis. (a) XRD patterns, (b) FTIR spectra, and (c) XPS spectra of B_2O_3, c-CNBMs, g-CNBMs, and y-CNBMs, respectively; (d-g) HR B 1s, C 1s, N 1s, and O 1s XPS spectra and the corresponding fitting curves of (i) c-CNBMs, (ii) g-CNBMs, and (iii) y-CNBMs, respectively. .

the stretching vibrations of the B-O bonds (*i.e.*, located at 1440 cm^{-1}) was also identified, demonstrating the dehydration of BA during the pyrolysis process. Moreover, a series of new characteristic peaks was observed. For instance, the absorption peaks at approximately 1024, 945, and 782 cm^{-1} were attributed to the bending vibrations of B-O-C, the stretching vibrations of B-C bonds, and the out-of-plane bending vibrations of the B-N-B structure, respectively [31,38,44]. These findings indicated that the dehydration covalent coupling reaction occurred between the carbon source and BA. The two broad absorption peaks located at 3440 and 3381 cm^{-1} were attributed to the stretching vibrations of the N-H/O-H bonds [31,38,44]. In addition, three absorption peaks located at 1630, 1400, and 1100 cm^{-1} were assigned to the stretching vibrations of the C=O/C=N, C-O, and C-N bonds, respectively [41,52]. These peaks demonstrated the carbonization of H-urea. More importantly, as the pyrolysis temperature increased, the intensity of the absorption peaks corresponding to C=O/C=N (1630 cm^{-1}) and C-O (1400 cm^{-1}) increased from the c-CNBMs to g-CNBMs and y-CNBMs, indicating that a higher pyrolysis temperature was beneficial for the carbonization of H-urea and the formation of CPDs or CQDs. These FT-IR results were further confirmed by XPS analysis. As a reference, only the B 1s and O 1s peaks were observed in the XPS spectrum of B_2O_3 (Fig. 3c), while the HR B 1s and O 1s spectra only exhibited peaks at B-O (194.0 eV) and O-B/O-H (533.0 eV), respectively (Fig. S6 in Supporting information) [44,48]. However, the full survey XPS spectra of these three materials exhibited four peaks at 192.1, 284.9, 401.2 and 532.1 eV, which were attributed to B 1s, C 1s, N 1s, and O 1s, respectively. Therefore, these materials contained the same elemental composition (*i.e.*, C, N, O and B) (Table S1 in Supporting information). The B/O ratios (*i.e.*, 0.55, 0.58 and 0.62) in the three materials gradually increased along with the pyrolysis temperature, indicating the promoted dehydration of BA. In the HR XPS spectra of each element, the B 1s spectrum was fitted into two peaks at 191.3 eV (B-C/B-N) and 192.4 eV (BCO_2) (Fig. 3d) [31,38,44,45]. The C 1s spectrum contained four peaks located at 284.8, 285.5, 286.0 and 288.0 eV, which could be identified as C-C/C=C, C-O, C-N, and C=O/C=N, respectively (Fig. 3e) [39,47]. The N 1s spectrum consisted of three peaks at 399.8, 401.4 and 402.2 eV, which corresponded to the C=N, N-H, and graphite N bonds, respectively (Fig. 3f) [41,52]. The O 1s spectra showed the existence of C-O/C=O bonds at 532.0 eV and O-B/O-H bonds at 533.0 eV (Fig. 3g) [31,32]. The corresponding fitting results are summarized in Table S2, which further provided a relatively quantitative alteration of the different bonds. Herein, the signal of BCO_2 (192.4 eV) means boron atoms being surrounded by carbon and oxygen atoms, revealing the presence of B_2O_3 [31,38,44,45]. Moreover, the emergence of B-C/B-N (191.3 eV) indicated the formation of covalent bonds between the B_2O_3 and CDs through the dehydration reaction, and these bonds could facilitate $n\rightarrow\sigma^*$ interactions for TSC emissions [38]. With increasing pyrolysis temperature, the BA molecules dehydrated to form B_2O_3, resulting in a decrease in B-C/B-N and an increase in BCO_2 bonds. More notably, when the pyrolysis temperature increased from 240 °C to 300 °C, the content of C obviously decreased (Table S1), which further revealed that more carbon sources were consumed at higher pyrolysis temperatures, resulting in the growth of the sp^2 hybrid structure *via* the dehydration, deamination, and carbonization reactions. All of these contributed to the obvious increase in C-O, C=O/C=N bonds and graphite N, and decrease in C-C/C=C, C-N, and N-H bonds (Table S2). In addition, CPDs and CQDs gradually formed in the g-CNBMs and y-CNBMs due to the relative higher pyrolysis temperature (*i.e.*, 260 and 300 °C, respectively). These observations were consistent with the FT-IR analysis, and TEM and HR TEM results discussed above.

To verify the origin of the ultralong and controlled RTP characteristics, the more in-depth photophysical properties of the materials were systemically investigated. First, the UV–vis absorption spectra were recorded. As shown in Fig. 4a, the UV–vis spectra of the materials displayed two major peaks at 280 and 340 nm, which were attributed to the $\pi\rightarrow\pi^*$ transitions of the C=C/C=N groups and the $n\rightarrow\pi^*$ transitions of C=O/C=N [41,52]. In addition, the intensities of the two absorption bands gradually increased with increasing pyrolysis temperature, indicating a higher carbonization degree and that more π-conjugate structures formed from the c-CNBMs into g-CNBMs and y-CNBMs. As shown in Fig. 4b and Fig. S7 (Supporting information), although the PL excitation spectra of

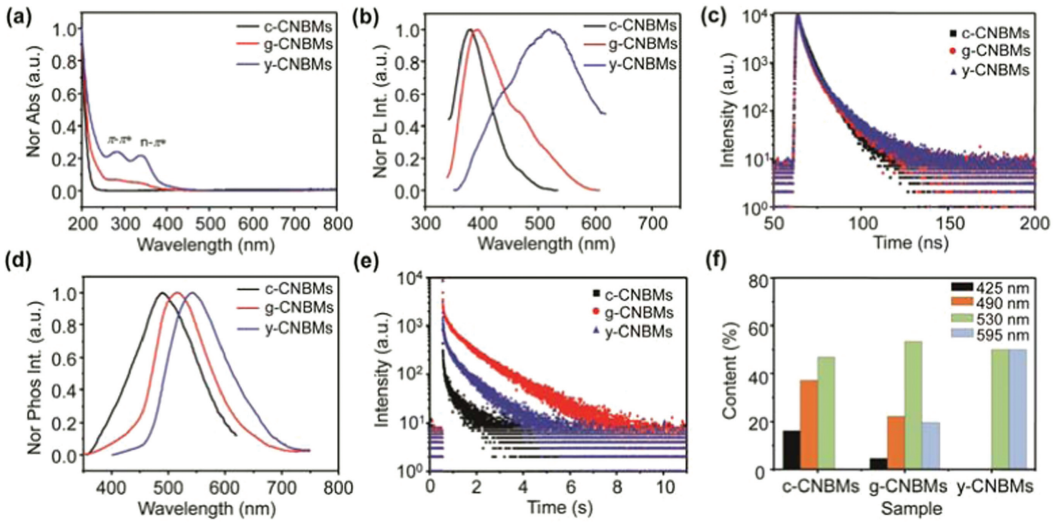

Fig. 4. Optical properties analysis. (a) UV–vis absorption spectra of c-CNBMs, g-CNBMs, and y-CNBMs. (b, c) PL emission (λ_{ex} = 340 nm) and decay (λ_{ex} = 320 nm) spectra of c-CNBMs, g-CNBMs, and y-CNBMs. (d, e) The afterglow emission and decay spectra of c-CNBMs, g-CNBMs, and y-CNBMs under a single excitation wavelength (λ_{ex} = 340 nm). (f) The RTP spectra of the three composites in (d), which were fitted by Gaussian functions (Fig. S7 in Supporting information), and the relative amplitudes of each fitted Gaussian peak are shown in (f).

all three materials were centered around 340 nm, their PL emission maxima gradually red-shifted from 390 nm to 400 nm, and to 520 nm with absolute PL quantum yields (QYs) of 2.76%, 5.95% and 4.95% (Table S3 in Supporting information), respectively. Notably, the emission bands of the c-CNBMs, g-CNBMs, and y-CNBMs gradually broadened, and the PL emission spectra of the three materials displayed excitation-wavelength-dependent emission behavior. These results indicated that multiple luminescent centers existed in these materials. According to their PL decay spectra, the PL lifetimes of the c-CNBMs, g-CNBMs, and y-CNBMs were determined to be 1.57, 2.28, and 2.52 ns, respectively (Fig. 4c and Table S4 in Supporting information). The differences in the PL lifetimes further confirmed the origin of the above-mentioned emissions from the multiple emissive centers [53,54]. More importantly, the RTP emission spectra of the three materials also displayed broad emission bands and significant red-shifting from 480 nm to 540 nm under a single excitation wavelength (λ_{ex} = 340 nm) (Fig. 4d). Moreover, RTP emission spectra of the three materials also displayed excitation-wavelength-dependent behavior (Fig. S1). Therefore, the RTP emissions of the three materials were similar to their PL, due to the presence of multiple emissive centers. However, from the time-resolved decay curves of the RTP emissions (Fig. 4e and Table S5 in Supporting information), the average afterglow lifetimes of the three materials were calculated to be 0.95–1.32 s, indicating their long-lived emission features. Moreover, the RTP emission spectra, shown in Fig. 4d, were analyzed by fitting with Guassian functions. As shown in Fig. S8 (Supporting information), all of these spectra could be fitted with multiple Gaussian peaks located at *ca.* 425, 490, 530, and 595 nm, corresponding to the different emissive centers. The emissive band percentages at 425 and 490 nm decreased with increasing pyrolysis temperature. By contrast, the emissive band percentages gradually increased at wavelengths of 530 and 595 nm (Fig. 4f and Table S6 in Supporting information). These changes were responsible for the shifts in the RTP emissions from c-CNBMs to g-CNBMs and to y-CNBMs. Furthermore, their excitation spectra (*i.e.*, c-CNBMs and g-CNBMs at 425 nm; c-CNBMs, g-CNBMs, and y-CNBMs at 490 nm and 530 nm; g-CNBMs and y-CNBMs at 595 nm) were also measured (Fig. S9 in Supporting information). The corresponding RTP excitation and UV–vis absorption spectra indicated that the shorter wavelength of RTP emission (*i.e.*, 425 nm) of c-CNBMs and g-CNBMs came from the n→σ^* transitions of B-C/B-N bonds and $\pi\rightarrow\pi^*$ transitions of the C=C/C=N relative groups, while the longer wavelength RTP emissions (*i.e.*, 490 nm, 530 nm and 595 nm) of g-CNBMs and y-CNBMs were mainly attributed to the n→π^* transitions produced by the C=O/C=N relevant structures. Notably, although the excitation of 340 nm did not exactly match the energy for the excitation of $\pi\rightarrow\pi^*$ transitions of the C=C/C=N groups, small parts of the 425 nm RTP from the c-CNBMs and g-CNBMs were also observed (Fig. 4f, Fig. S8 and Table S5), due to contributions from the n→π^* transitions of the C=O/C=N groups. With increasing pyrolysis temperature, more C=O/C=N groups formed; therefore, the percentages of long-wavelength RTP increased and the three composites showed multicolor RTP under single wavelength excitation (340 nm).

Based on the above characterizations and analyses, the formation process and multicolor RTP alteration mechanism of c-CNBMs, g-CNBMs, and y-CNBMs could be tentatively proposed as follows. The H-urea and BA first underwent dehydration condensation under heating (240 °C) to form nonconventional luminophores (oligomers from slight crosslinking). Then, luminescent polymer clusters were produced through further dehydration and crosslinking among these oligomers. Meanwhile, carbonization started to occur with increasing reaction temperature (260 °C), leading to the production of CPDs with a low crystallization degree. When the temperature was further elevated (300 °C), CQDs with more compact structures formed by the emerging larger crystalline regions and higher crystalline degree in the interiors of the dots. In this process, carbon sources were gradually consumed, which was accompanied by the dehydration of BA. Therefore, the nonconventional luminophores, CPDs and CQDs, were uniformly dispersed and embedded in the B_2O_3 matrix. All of the composites could stabilize the T1 species and suppress the non-radiative relaxation processes of the excited triplet excitons, thus generating efficient RTP emissions. Moreover, during pyrolysis treatment, some B atoms were covalently coupled with the C and N atoms, forming covalent bonds (*i.e.*, B-C and B-N bonds), which may have promoted the n→σ^* transitions, triggering the construction of inter/intramolecular TSC [38]. TSC could form a narrow energy band and effectively populate the triplet excitons by overcoming the weak SOC of the n→σ^* transitions; thus, contributing to the RTP emissions around 425 nm. Moreover, Gaussian fitting indicated

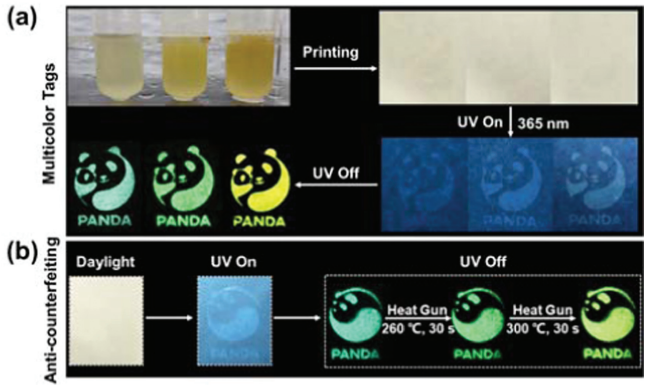

Fig. 5. Applications of the c-CNBMs, g-CNBMs, and y-CNBMs in information security. (a) Multicolor RTP inks and tags. (b) c-CNBMs based thermo-stimuli-responsive polychrome RTP ink for high-security level anti-counterfeiting.

that the $\pi \rightarrow \pi^*$ transitions of C=C/C=N also contributed to the RTP emission of 425 nm and the RTP emission peaks of 490, 530 and 595 nm were mainly derived from the $n \rightarrow \pi^*$ transitions of C=O/C=N relevant structures. Consequently, all the emitting centers (*i.e.*, C-B, B-N, C=C, C=O, and C=N relevant structures) were responsible for the RTP emissions of these materials. With the alteration of pyrolysis temperature, the contents of certain types of bonds relevant structures would dominate the RTP process, thus, showing color-tunable RTP emissions.

The three materials showed great potential for information security applications due to their outstanding stability (Fig. S11 in Supporting information) and temperature dependent color-tunable RTP features. To demonstrate such an application, a tag (a panda picture) was printed onto a piece of common A4 paper *via* silk-screen printing using the three material-based inks (see experimental section for details in Supporting information). After completely drying, the colorless patterns were obtained under ambient conditions (Fig. 5a). Under the irradiation of a 365 nm UV lamp, only weak panda pattern was observed due to the strong PL background of the A4 paper. After the excitation light was removed, cyan, green, and yellow RTP were observed for several seconds (Fig. 5a and Fig. S10 in Supporting information). More impressively, the c-CNBMs were used to fabricate thermo-stimuli-responsive polychrome security inks for high-security level anti-counterfeiting and advanced information encryption applications. As shown in Fig. 5b, when the pattern printed by the c-CNBMs inks was treated by heating with a heat gun (260 °C for 30 s), it was still invisible under daylight and was blue, however, its RTP colors changed from cyan to green after the UV lamp was turned off. When the heating treatment reached 300 °C (for 30 s), the RTP emissions of this pattern further evolved into yellow when UV excitation stopped. To the best of our knowledge, this type of color tunable RTP feature has rarely been reported thus far [31,32]. In addition, the changeable colors could be easily distinguished by the naked eye due to their long duration. Therefore, all of these advantages were beneficial for high-security anti-counterfeiting in daily life. These results also demonstrated that the reported materials with controllable RTP color features were promising for anti-counterfeiting applications for protecting the authenticity of many valuable items, such as banknotes, tickets, coupons, and lotteries, as well in security fields for the encryption of important information, such as codes, messages, and security tags.

In summary, we reported on a facile strategy to prepare color-tunable RTP materials by controlling the pyrolysis temperature of H-urea and BA. Based on the structural investigations and photophysical analysis, we proposed that the tunable RTP colors originated from the formation of multiple luminescent centers, which were embedded *in-situ* in a matrix during the pyrolysis process. More interestingly, the material prepared at a lower temperature (*i.e.*, c-CNBMs) exhibited a unique thermo-stimuli-responsive color-changeable RTP character. Based on their remarkable optical features, these materials demonstrated that they could be useful in the fields of advanced anti-counterfeiting and information protection. This study provided a facile method for the preparation of color-tunable metal-free RTP materials with long-lasting emissions. Furthermore, we believe that this luminescent center engineering and *in-situ* immobilization strategy could offer new opportunities for designing thermo-stimuli-responsive smart materials for high-level information security, anti-counterfeiting, and multiplexed storage.

Declaration of competing interest

The authors declare that they have no known competing financial interests or personal relationships that could have appeared to influence the work reported in this paper.

Acknowledgments

The authors acknowledge the National Natural Science Foundation of China (Nos. 51872300 and 52003284), the Natural Science Foundation of Jiangsu Province (No. BK20210481), and the Fundamental Research Fund of Jiangnan University (No. JUSRP122015) for financially supporting this work.

Supplementary materials

Supplementary material associated with this article can be found, in the online version, at doi:10.1016/j.cclet.2022.107950.

References

[1] M. Yu, M.H. Saeed, S. Zhang, et al., Adv. Funct. Mater. 32 (2022) 2109472.
[2] H.Q. Yin, X.B. Yin, Small 18 (2022) 2106587.
[3] Y. Wu, W. Wu, Adv. Opt. Mater. 9 (2021) 2100281.
[4] E. Nannen, J. Frohleiks, S. Gellner, Adv. Funct. Mater. 30 (2020) 1907349.
[5] J.Q. Liu, Z.D. Luo, Y. Pan, et al., Coordin. Chem. Rev. 406 (2020) 213145.
[6] P. Dang, D. Liu, G. Li, et al., Adv. Opt. Mater. 8 (2020) 1901993.
[7] J. Zhou, Q. Liu, Z. Xia, J. Mater. Chem. C 6 (2018) 4371–4383.
[8] X.P. He, X.L. Hu, T.D. James, et al., Chem. Soc. Rev. 46 (2017) 6687–6696.
[9] F. Nie, B. Zhou, K.Z. Wang, D. Yan, Chem. Eng. J. 430 (2022) 133084.
[10] Y. Wang, H. Gao, J. Yang, et al., Adv. Mater. 33 (2021) 2007811.
[11] J. Tan, Q. Li, S. Meng, et al., Adv. Mater. 33 (2021) 2006781.
[12] H. Jin, X. Jiang, Z. Sun, R. Gui, Coordin. Chem. Rev. 431 (2021) 213694.
[13] X. Wang, H. Ma, M. Gu, et al., Chem. Mater. 31 (2019) 5584–5591.
[14] Z. He, H. Gao, S. Zhang, et al., Adv. Mater. 31 (2019) 1807222.
[15] N. Gan, H. Shi, Z. An, W. Huang, Adv. Funct. Mater. 28 (2018) 1802657.
[16] A. Forni, E. Lucenti, C. Botta, E. Cariati, J. Mater. Chem. C 6 (2018) 4603–4626.
[17] Z. Wang, H. Yuan, Y. Zhang, et al., J. Mater. Sci. Technol. 101 (2022) 264–284.
[18] S. Hirata, Adv. Opt. Mater. 5 (2017) 1700116.
[19] W. Zhao, Z. He, J.W.Y. Lam, et al., Chem 1 (2016) 592–602.
[20] S. Xu, R. Chen, C. Zheng, W. Huang, Adv. Mater. 28 (2016) 9920–9940.
[21] S. Guo, W. Dai, X. Chen, et al., ACS Mater. Lett. 3 (2021) 379–397.
[22] W. Jia, Q. Wang, H. Shi, et al., Chem. Eur. J. 26 (2020) 4437–4448.
[23] Z. An, C. Zheng, Y. Tao, et al., Nat. Mater. 14 (2015) 685–690.
[24] F. Gu, X. Ma, Chem. Eur. J. 28 (2022) e202104131.
[25] L. Yuan, Y. Jin, Y. Su, et al., Laser Photonics Rev. 14 (2020) 2000123.
[26] L. Huang, C. Qian, Z. Ma, Chem. Eur. J. 26 (2020) 11914–11930.
[27] D. Li, J. Yang, M. Fang, et al., Sci. Adv. 8 (2022) 8392–8400.
[28] L. Gu, H. Shi, L. Bian, et al., Nat. Photon. 13 (2019) 406–411.
[29] P. Gao, Z. Xie, M. Zheng, Chin. Chem. Lett. 33 (2022) 1659–1672.
[30] X. Yang, X. Li, B. Wang, et al., Chin. Chem. Lett. 33 (2022) 613–625.
[31] Y. Ding, X. Wang, M. Tang, H. Qiu, Adv. Sci. 9 (2022) 2103833.
[32] Z. Wang, J. Shen, B. Xu, et al., Adv. Opt. Mater. 9 (2021) 2100421.
[33] S. Zhu, Y. Song, J. Shao, et al., Angew. Chem. Int. Ed. 54 (2015) 14626–14637.
[34] S. Zhu, L. Wang, N. Zhou, et al., Chem. Commun. 50 (2014) 13845–13848.
[35] S. Tao, T. Feng, C. Zheng, et al., J. Phys. Chem. Lett. 10 (2019) 5182–5188.
[36] S. Tao, S. Lu, Y. Geng, et al., Angew. Chem. Int. Ed. 57 (2018) 2393–2398.
[37] S. Zhu, Y. Song, X. Zhao, et al., Nano Res. 8 (2015) 355–381.
[38] C. Zhang, H. Wang, X. Lan, et al., J. Phys. Chem. Lett. 12 (2021) 1413–1420.
[39] S. Tang, T. Yang, Z. Zhao, et al., Chem. Soc. Rev. 50 (2021) 12616–12655.
[40] K. Jiang, S. Hu, Y. Wang, et al., Small 16 (2020) 2001909.
[41] Q. Li, M. Zhou, Q. Yang, et al., Chem. Mater. 28 (2016) 8221–8227.

[42] K. Jiang, L. Zhang, J. Lu, et al., Angew. Chem. Int. Ed. 55 (2016) 7231–7235.
[43] Y. Deng, D. Zhao, X. Chen, et al., Chem. Commun. 49 (2013) 5751.
[44] Z. Zhou, Z. Song, J. Liu, et al., Adv. Opt. Mater. 10 (2022) 2100704.
[45] W. Li, W. Zhou, Z. Zhou, et al., Angew. Chem. Int. Ed. 58 (2019) 7278–7283.
[46] J. Zhao, W. Wu, J. Sun, S. Guo, Chem. Soc. Rev. 42 (2013) 5323–5351.
[47] D.N. Congreve, J. Lee, N.J. Thompson, et al., Science 340 (2013) 334–337.
[48] Z. Zhou, K. Jiang, N. Chen, et al., Mater. Lett. 276 (2020) 128226.
[49] C. Zheng, S. Tao, Y. Liu, et al., Chin. Chem. Lett. 33 (2022) 4213–4218.
[50] Y. Zhai, P. Wang, X. Zhang, et al., Chin. Chem. Lett. 33 (2022) 783–787.
[51] Y. Wu, X. Fang, J. Shi, et al., Chin. Chem. Lett. 32 (2021) 3907–3910.
[52] B. Zhao, R. Yu, K. Xu, et al., J. Mater. Chem. C 9 (2021) 15577–15582.
[53] L. Pan, S. Sun, A. Zhang, et al., Adv. Mater. 27 (2015) 7782–7787.
[54] Y. Wang, S. Kalytchuk, Y. Zhang, et al., J. Phys. Chem. Lett. 5 (2014) 1412–1420.